Dependence of domain wall dynamics on background wave number

Carina Kamaga, Denis Funfschilling,* and Michael Dennin
Department of Physics and Astronomy, University of California at Irvine, Irvine, California 92697-4575, USA
(Received 25 April 2003; published 28 January 2004)

We report on the growth of domains of standing waves in electroconvection in a nematic liquid crystal, focusing on the evolution of domain walls. An ac voltage is applied to the system, forming an initial state that consists of traveling striped patterns with two different orientations, zig and zag rolls. The standing waves are generated by suddenly applying a periodic modulation of the amplitude of the applied voltage that is approximately resonant with the traveling frequency of the pattern. By varying the modulation frequency, we are able to vary the steady-state, average wave number. We characterize the evolution of the domain walls as a function of the average background wave number by measuring the total area and length of domain walls present in the system as a function of time. We find that as the background wave number is varied away from the ''natural'' wave number for the pattern, the evolution of the domain walls occurs at a faster rate.

DOI: 10.1103/PhysRevE.69.016308 PACS number(s): 47.54.+r, 64.60.Cn

I. INTRODUCTION

Our understanding of the role of the interaction between defects and a periodic background during the ordering of patterned systems after a sudden quench remains limited. Simulations of the growth of striped domains clearly point to the importance of understanding the interaction between defects and the background wave number [1–4]. Yet, experimental studies are limited [6,5,7], and there is no general theoretical understanding of the problem. The generic problem of the response of a system to a sufficiently large, sudden change of an external parameter, referred to as a quench, arises in many materials situations, such as magnetic materials, alloys, binary fluids, polymer blends, and liquid crystals [8]. Generally, one is interested in the case where an initially uniform state loses stability after the quench. When there is more than one possibility for the new state (such as spin up or down in a magnetic system), domains form. These domains coarsen, or grow, as a function of time, a process that is often referred to as *domain coarsening* or *phase ordering*. The dynamics of phase ordering for the special case of uniform domains is relatively well understood [8]. In general, such domains are characterized by a single length scale $l(t)$ that grows according to a power law $l(t) \sim t^n$. Here n is referred to as the *growth exponent*. For systems with a nonconserved order parameter $n = 1/2$. Systems with a conserved order parameter have $n = 1/3$. Generally, these exponents can be understood in terms of the topological defects of the relevant order parameter [8]. In contrast, for patterned domains, there is no general explanation of the observed growth exponents, in terms of the topological defects or otherwise. However, specific examples clearly point to the importance of the topological defects [1–5]. One finds that there are two main complications when considering the coarsening of patterned domains: (1) the interaction between the defects and the periodic background, and (2) the additional length scale that is set by the periodicity of the pattern. In this paper, we focus on the issue of the impact of the background wave number on the dynamics of topological defects.

For systems in which the domains are composed of stripes, theoretical studies of the power-law scaling of the late-time domain growth has focused on simulations and analysis of the Swift-Hohenberg equation [1–4,9–12]. Experiments have been performed in both a thermodynamic system, diblock copolymers [5,6], and a driven system, electroconvection [7]. In this paper, we will refer to *thermodynamic* quenches, or systems, as ones where the asymptotic state after the quench is one of thermodynamic equilibrium. *Driven* systems refer to ones in which the asymptotic state is not an equilibrium state, but it is a steady state of the system. Typically, both the simulations and experiments consider measurements of the structure factor $S(k)$. An important aspect of such measurements is the fact that the width of the relevant peaks in the structure factor is a measure of both variations in wave number and domain size. Therefore, information about the two important lengths scales are mixed in a nontrivial way. Various other measures of the domain growth that do not contain information about the wave number have been studied. These include orientational correlation functions for the wave vector field, defect densities, and domain-wall lengths. All of these measures probe only the domain size.

In both simulations and experiments, the changes in the width of the structure factor occur at a significantly slower rate than changes in the other measures. In numerical simulations, growth exponents that are determined from measurements of $S(k)$ are consistent with $n = 1/5$ [1,10]. In contrast, measurements based on orientational correlation functions exhibit a model dependence. Simulations of a version of the Swift-Hohenberg model that has a potential are consistent with a growth exponent $n = 1/4$, but the nonpotential case gives $n = 1/2$ [1]. The two experimental measures of striped domain growth are consistent with the simulation results for the potential case. The orientational correlation function and defect densities have been measured experimentally in diblock copolymers [6], giving $n = 1/4$. For electroconvection, it was found that the growth exponent measured using

*Present address: Department of Physics, University of California at Santa Barbara, Santa Barbara, CA 93106, USA.

$S(k)$ is consistent with $n=1/5$ and measurement of the domain size using total domain-wall length gave $n=1/4$ [7]. These experiments clarified that the differences in growth exponents between $S(k)$ and other measures could be explained by considering the evolution of the local wave number distribution, which is found to dominate the width of $S(k)$ at late times [7].

The issue of the interaction between defects and the background periodicity is apparent in various features of domain growth, as revealed in simulations. First, domain growth is observed to be affected by strong pinning of grain boundaries by the periodic background [2,11]. Because the pinning strength is related to the amplitude of the pattern, the measured growth exponents can depend on the depth of the quench. A related issue is that the growth exponents are also found to depend on the level of noise in the system [9,12]. This is attributed to the fact that noise can provide a source of ''depinning'' for the defects. Finally, the difference in the average wave number for the potential and nonpotential versions of the Swift-Hohenberg equations has been proposed as one possible explanation of the different scaling exponents for the orientational correlation function [1]. Recent simulations using a different model of stripe formation (the nonlinear phase model) have shown that different classes of defects can lead to different growth exponents [4]. These same simulations suggest that the domain-wall width and length evolve with different scaling in time [4], suggesting yet another possible length scale in the problem.

In this paper, we report on a systematic, experimental study of the impact of changes in the average wave number on the growth of domains in which we find that the domain growth occurs at a faster rate as the wave number is tuned away from the ''natural'' wave number. This provides a useful test of the proposed explanation, based on the background wave number, for different growth rates that are observed in two versions of the Swift-Hohenberg equation [1]. In particular, the growth of domains in the simulation also was faster when the system was not at the ''natural'' wave number [1]. An important feature of the experiments is that we can tune the wave number over a range of values, instead of just the two wave numbers considered in the simulations [1]. Furthermore, we report on measurements of the behavior of the domain-wall length and area that are compared with simulations reported in Ref. [4]. The system we use is electroconvection in the nematic liquid crystal I52 [13,14]. A nematic liquid crystal is a fluid in which the molecules are aligned on average [15]. The axis along which the average alignment points is referred to as the director. For electroconvection [16], a nematic liquid crystal is placed between two glass plates that have been treated so that the director is everywhere parallel to the plates. An ac voltage is applied perpendicular to the plates. Above a critical value of the voltage, a pattern of stripes forms. Because the system is anisotropic (the director selects a preferred axis), the states are usually characterized by the angle between the wave vector of the pattern and the undistorted director θ. States with the same wave number and angle $\pm\theta$ are degenerate and referred to as zig and zag, respectively. For the system discussed in this paper, the initial pattern consists of four traveling stripe states [17]; right- and left-traveling zig and zag rolls. It has been established for this system that above a critical value for a modulation of the applied voltage at twice the traveling frequency, the system consists of either standing zig or zag rolls [14]. Therefore, a sudden quench of the system from below this critical value to above it results in the nucleation of domains of standing zig and zag rolls, which proceed to coarsen. The dominant topological defects in the system are domain-walls between the domains of zig and zag rolls. We will focus on the evolution of these domain-walls.

As discussed above, measurements of growth exponents for this system have focused on quenches that used exactly twice the traveling frequency. This results in domains with the natural wave number for the pattern. Reference [7] reports a value of $n=1/4$ for the growth of the domain size, based on measurements of the domain-wall dynamics, and $n=1/5$ for the scaling of $S(k)$. A single initial experiment for a modulation frequency slightly different from twice the traveling frequency suggested similar behavior. However, a systematic exploration of changes in the wave number, by varying the modulation frequency, is possible for this system [14], and was not carried out at the time. In this paper, we report on such a study. The rest of the paper is organized as follows. Section II provides the details of the experimental system and the techniques used to analyze the domain growth. Section III presents the results of the experiment. Section IV provides a discussion of the results.

II. EXPERIMENTAL DETAILS

We used the liquid crystal I52 [18] doped with iodine. Due to the nature of I52, 8% iodine by weight was used initially. However, a significant fraction of the iodine evaporates before the cells are filled, so the final concentration is not well controlled. We used commercial liquid crystal cells [19] composed of two transparent glass plates coated with a transparent conductor, indium-tin oxide. The cells were 2.54×2.54 cm^2, with the conductor forming a square 1×1 cm^2 in the center of the cell. The glass was also treated with a rubbed polymer to obtain uniform planar alignment of the director. We define the direction parallel to the undistorted director to be the x axis and the direction perpendicular to the undistorted director to be the y axis.

The apparatus is described in detail in Ref. [20]. It consists of an aluminum block with glass windows. The temperature of the block was kept constant to ±0.001 °C. Polarized light is applied from the bottom of the cell. Above the cell, there is a charge-coupled device camera to capture the image of patterns using the standard shadowgraph technique [21].

We apply an ac voltage of the form $V(t)=\sqrt{2}[V_o+V_m\cos(\omega_m t)]\cos(\omega_d t)$ perpendicular to the glass plates. Here V_o is the amplitude of the applied voltage in the absence of modulation, V_m is the modulation amplitude, ω_m is the modulation frequency, and ω_d is the driving frequency. For all of the experiments reported on here, $\omega_d/2\pi=25$ Hz. The critical voltage V_c is defined as the value of V_o for which the system makes a transition from a uniform state

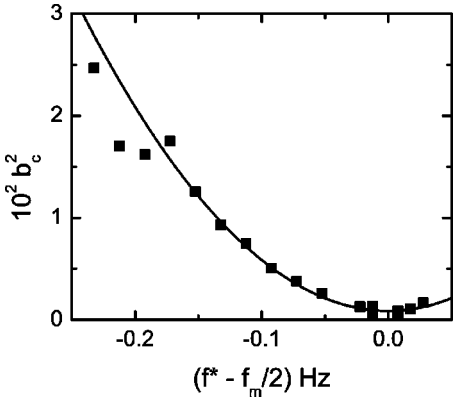

FIG. 1. Onset value for standing waves (b_c) at a value of $\epsilon=0.04$ as a function of $\delta f = f^* - f_m/2$. Here f^* is the natural travel frequency of the pattern at $\epsilon=0.04$ and f_m is the modulation frequency. The parameter b_c is the critical value of $b = V_m/V_c$. Here V_m is the modulation voltage and $V_c = 16.6$ V is the critical voltage for the onset of a pattern in the absence of any modulation. The solid line is a fit to the data used to determine $f^* = 0.26 \pm -0.01$ Hz.

to the superposition of traveling rolls *in the absence of modulation*. For the studies reported on here, $V_c = 16.6$ V. There are two relevant control parameters: $\epsilon = (V_o/V_c)^2 - 1$ and $b = V_m/V_c$.

For the experiments discussed here, the system is initially at $\epsilon=0.04$ and $b=0$, i.e., above onset with no modulation. This corresponds to $V_o = 17.0$ V. As mentioned in Sec. I, there are only four modes needed to describe the observed convection rolls: zig and zag, right- and left-traveling oblique rolls. This state is an example of spatiotemporal chaos in that the amplitude of the four modes varies irregularly in space and time [22]. For each ϵ and ω_m, there exists a critical value of b, b_c, above which the system consists of standing zig and zag rolls. A quench corresponds to a sudden change of b to some value $b > b_c$. At and below V_c, the modulation frequency with the strongest coupling to the pattern, and correspondingly smallest value of b_c, is twice the Hopf frequency ω_h. The Hopf frequency is the traveling wave frequency at V_c. As one increases ϵ, the natural frequency of the pattern shifts. Because we worked at a finite value of ϵ, the smallest value of b_c occurs for a modulation frequency $\omega_m = 2\omega^*$, where ω^* is the natural frequency of the pattern at the given value of ϵ. Because it is the relative shift in frequency that matters, we will consider the behavior as a function of $\delta f = f^* - f_m/2$, where $f^* = \omega^*/2\pi$ and $f_m = \omega_m/2\pi$. For all experiments considered here, the natural frequency was $f^* = 0.26 \pm 0.01$ Hz. Figure 1 is a plot of b_c as a function of δf for $\epsilon=0.04$. We focus almost exclusively on the negative values of δf because for $\delta f > +0.01$ Hz, the pattern stabilized by modulation is standing waves that are a superposition of zig and zag rolls, and not individual domains of standing zig and zag rolls.

Quenches were performed for a range of δf. The final value of b in each case was selected so that the quench depths all corresponded to $\Delta b = 0.02$, as measured from the onset of standing waves (solid curve in Fig. 1). The camera was triggered to take the images at the same point in the modulation cycle. This ensured that the pattern was imaged at the same point in the standing wave cycle. Each image covered a region of 4.1×3.1 mm^2 of the cell. Time is scaled by the director relaxation time $\tau_d \equiv \gamma_1 d^2/(\pi^2 K_{11}) = 0.2$ s. Here γ_1 is a rotational viscosity, K_{11} is the splay elastic constant, and d is the thickness of the cell.

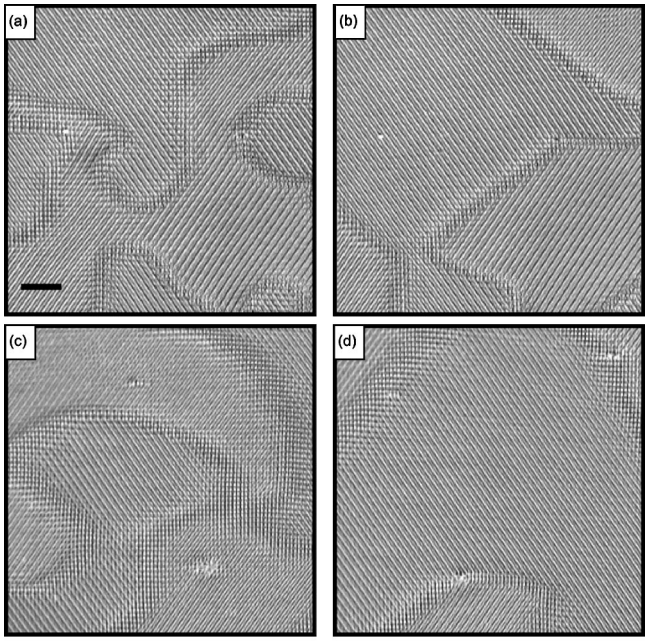

FIG. 2. Four images of domain growth. Images (a) and (b) are with a modulation frequency $\delta f = 0.008$ Hz, at $t = 96$ s and $t = 600$ s after the quench, respectively. Images (c) and (d) are with a modulation frequency $\delta f = -0.072$ Hz, at $t = 112$ s and $t = 700$ s after the quench, respectively. The solid bar in (a) is 0.2 mm.

An example of a small region of the pattern after a quench is given in Fig. 2. Two different quenches are illustrated: $\delta f = 0.008$ Hz and $\delta f = -0.072$ Hz. The images illustrate the type of patterns on which we focused: standing zig and zag rolls separated by domain-walls. The domain-walls clearly consist of the superposition of zig and zag rolls. For significantly larger values of δf, there is qualitatively different behavior. Regions of superposition that are ''domains'' in their own right appear. Further increasing $|\delta f|$ results in patterns that are entirely the superposition of zig and zag rolls, as existed for $\delta f > 0.01$ Hz. Though interesting, in these patterns the defects are no longer domain-walls, but localized defects. Future work will consider in more detail this other class of patterns.

In order to quantify the domain-wall dynamics, we converted the images to a scaled image of zig and zag domains, referred to as the *angle map*. This was done using the procedure detailed in Ref. [7]. Briefly, the local angle of the wave number is computed using the algorithm reported in Ref. [23]. This is used to produce an image with black and white domains representing regions of zig and zag, respectively. Regions of superposition of zig and zag rolls (the domain-walls) are represented by gray. Figure 3 illustrates a typical image [Fig. 3(a)] and the results after conversion to

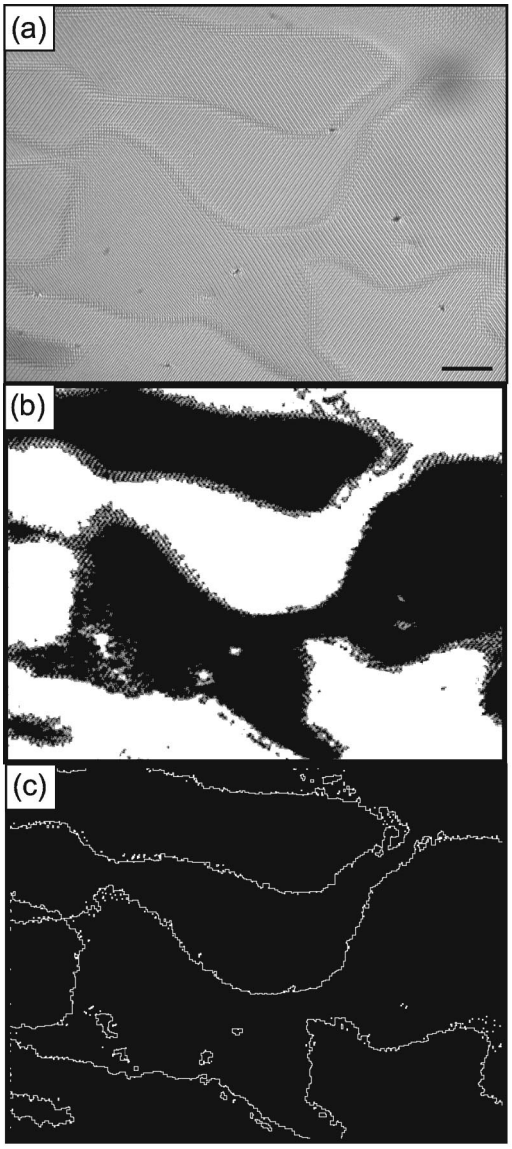

FIG. 3. (a) Image taken 384 s after a quench with $\delta f = 0.008$ Hz. (b) The same image converted to an "angle" map. The black and white regions are zig and zag rolls, respectively. The gray regions are the boundaries between domains. (c) The same image processed to highlight only the domains boundaries (white). The scale bar in (a) represents 0.4 mm.

an angle map [Fig. 3(b)]. Two measures of domain-wall size are used.

First, the normalized area of the domain wall A is considered. This quantity is proportional to the energy associated with the domain-wall. A is defined as the total number of gray pixels in the angle map divided by the total area of the viewing image. The area of the domain-wall will scale as $A \sim wl/l^2 = w/l$, where w is the width of the domain-wall and l is a typical length scale for a domain. For a constant domain-wall width, this quantity scales as the inverse of a characteristic domain size. If the domain-wall width scales differently than the typical domain size, a direct measure of the domain-wall length allows one to extract the scaling of the domain-wall width [4].

In order to directly measure the domain-wall width, we converted the angle map image to an image of the domain boundaries. An example of the result is shown in Fig. 3(c). This was a two step process. First, we reprocessed the angle map images so all the boundary pixels were associated with either a zig or zag domain, producing a black and white image. Then, a standard edge detection filter from the IMAQ Vision package [24] was used to find the boundaries between the domains. These boundaries are a single pixel wide, so the total number of boundary pixels gives the length of the domain-wall. We tested a number of different algorithms for associating boundary pixels with a zig or zag domain, including either associating all the boundary pixels with zig domains or all the pixels with zag domains. The details for associating a boundary pixel with a domain did not significantly change the determination of the domain-wall length. We considered the total domain-wall length per viewing area L. For this measure, $L \sim l/l^2 = l^{-1}$. By comparing A and L, we are able to obtain information about w.

The power spectrum, $S(k)$, of each image was computed. This was used to determine the average wave number $[\langle k \rangle \equiv \int kS(k)dk / \int S(k)dk]$ for the zig and zag rolls. In addition, we considered two other measures of the domain growth in order to make contact with previous measurements. The widths of the fundamental peak in $S(k)$ in both the x (σ_x) and y (σ_y) directions were determined using the second moment of $S(k)$. This gives $\sigma_x \equiv \sqrt{\langle k_x^2 \rangle - \langle k_x \rangle^2}$, with $\langle k_x^2 \rangle \equiv \int k_x^2 S(k)dk / \int S(k)dk$, and a similar definition for σ_y. (Note all of the integrals were taken as sums over a finite region around the fundamental peak, as described in Ref. [7].) σ_x and σ_y contain information about the typical size of a domain and the distribution of wave numbers in the respective directions. We also considered the width of the power spectrum of the angle map image $S(q)$. We use q to distinguish between the power spectrum of the angle map case and the power spectrum of the pattern itself. In this case, the peak is centered at $q=0$, as the angle map domains are uniform. Therefore, the width of the peak is related to the typical domain size only. Again, we separately considered the width in the x direction (w_x) and y direction (w_y), where the widths are defined in the same manner as for $S(k)$.

III. RESULTS

Figure 4 shows the time evolution of the average wave number (normalized by the critical wave number $k_c = 0.17\ \mu\text{m}^{-1}$) ($\langle k \rangle / k_c$) for the different quenches of interest. A number of features of the evolution are evident. First, as claimed, the late-time value of the $\langle k \rangle$ is dependent on δf [see Fig. 4(a)]. However, the wave number never reaches a constant value. For all quenches, the evolution after $t/\tau_d \approx 1000$ is consistent with a very slow logarithmic growth: $\langle k \rangle / k_c = a \log_{10}(t/\tau_d) + b$, with $a \approx 0.01$. This is illustrated in Fig. 4(b). There is a weak dependence on when the logarithmic growth begins (with values ranging from $2.7 < \log_{10}(t/\tau_d) < 3.1$) and on the coefficient (a) of the logarithmic growth [with values ranging from 0.006 to 0.02]. In general, for larger $|\delta f|$, evolution consistent with logarithmic time dependence occurs at a later time.

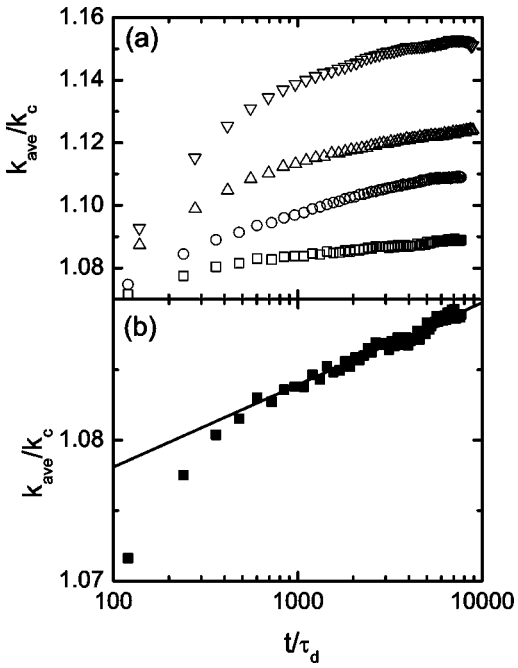

FIG. 4. (a) Average wave number (normalized by the critical wave number) for the zig standing rolls as a function of time after the quench. Time is scaled by the director relaxation time, τ_d. The symbols are as follows: (□) $\delta f = 0.008$ Hz, (○) $\delta f = -0.012$ Hz, (△) $\delta f = -0.022$ Hz, and (▽) $\delta f = -0.072$ Hz. The wave number for the zag rolls shows similar behavior. (b) An expanded view of the average wave number for $\delta f = 0.008$ Hz. The solid line is a guide to the eye illustrating the regime where the evolution of $\langle k \rangle$ is consistent with logarithmic growth in time.

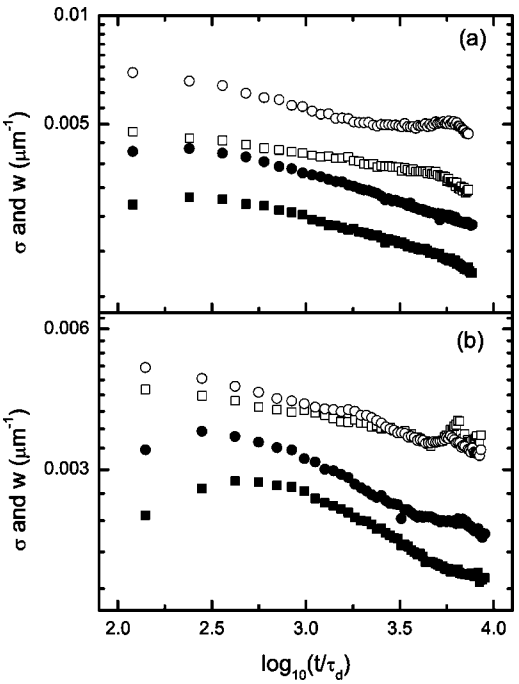

FIG. 5. Width of the power spectrum as a function of time for two different values of δf. Time is scaled by the director relaxation time τ_d. (a) $\delta f = 0.008$ Hz, (b) $\delta f = -0.072$ Hz. In both cases, the open symbols are for the power spectrum computed on the image with the stripes, with σ_x given by the squares and σ_y given by the circles. The closed symbols are for the power spectrum of the image of the angle map, with w_x given by the squares and w_y given by the circles.

Figure 5 shows the evolution of the width of the power spectrum for both the pattern (σ_x and σ_y) and the angle map (w_x and w_y) for two values of δf. There are a number of features that become apparent in these plots. First, initially the widths of peaks derived from the pattern and the angle map are on the same order of magnitude, within a factor of 2 or 3. This is a reflection of the fact that the initial domain sizes are on the same order as the variation in local wave number. Though as expected, σ_x and σ_y are larger than w_x and w_y. As the pattern evolves, the width of the peaks derived from the angle map become smaller. Ultimately, the widths based on the angle map reflect the fact that only a few domains are present in the image. In contrast, the widths of the peaks based on images of the pattern do not change nearly as much. This reflects the slow changes in the variation of the local wave number that come to dominate $S(k)$ at late times. This difference is consistent with earlier results comparing $S(k)$, which includes information about the variation in local wave number, to more direct measures of the domain size [1,7].

One can quantify the different rates of change of the two measures in Fig. 5 by fitting the data to a power law, $\sigma \sim t^n$ or $w \sim t^n$, and determining the growth exponent n. One finds that growth exponents based $S(k)$ are smaller than those based on $S(q)$. For late times, assuming $\sigma \sim t^n$, the exponents n are on the order of 0.1. In contrast, for w_x and w_y, one obtains growth exponents of $n = 0.2$ or larger. One can see in Fig. 5 that the evolution of $S(q)$ is faster for $\delta f = -0.072$ than it is for $\delta f = 0.008$, and this is reflected in a roughly doubling of the value of n. One can also use these exponents to test for strong anisotropy in the growth. The examples in Fig. 5 illustrate the fact that w_x and w_y have different magnitudes initially, but similar time dependence. This suggests that even though the domains are initially anisotropic, the degree of anisotropy is relatively constant in time. This is apparent in the spatial images where one does not observe long, skinny domains at later times, as would happen if the growth itself was highly anisotropic. Similar behavior is observed for σ_x and σ_y. This result justifies our assumption of a single length scale $[l(t)]$ associated with the domain size that is used for analyzing the domain-wall properties.

As noted above, there are only a few domains present in the image at late times. Therefore, the measures of the domain size based on the widths of the peaks in $S(k)$ and $S(q)$ are limited by finite size effects and limited resolution. Because of these potential sources of error, the exponents are not being quoted as proof of a scaling regime. They are provided simply as a quantitative measure of the obvious differences in temporal evolution evident in Fig. 5. A better measure of the rate of domain growth is obtained by our measurements of the domain-wall dynamics directly. For these measures, there is sufficient total domain-wall length present in the system that we can reliably measure the rate of

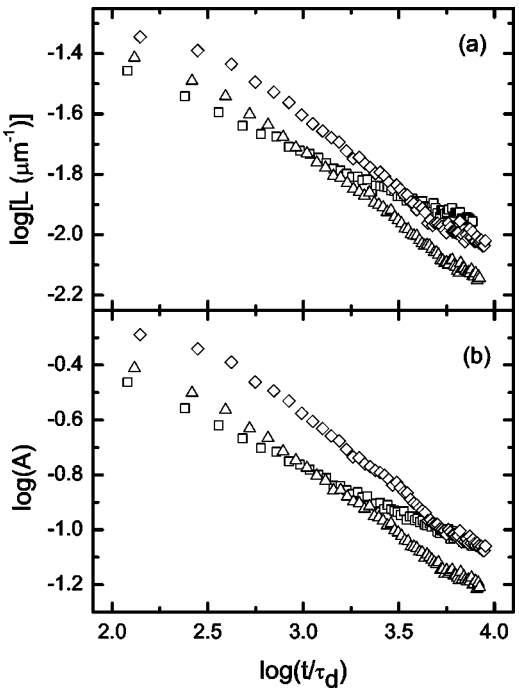

FIG. 6. (a) Total normalized domain-wall length (L) as a function of time. Time is scaled by the director relaxation time τ_d. The symbols are as follows: (□) $\delta f = 0.008$ Hz, (△) $\delta f = -0.022$ Hz, and (◇) $\delta f = -0.072$ Hz. (b) Total normalized domain-wall area (A) as a function of time. Time is scaled by the director relaxation time τ_d. The symbols are as follows: (□) $\delta f = 0.008$ Hz, (△) $\delta f = -0.022$ Hz, and (◇) $\delta f = -0.072$ Hz.

change of the domain-wall length during the time we monitored the growth.

The results for the direct measurements of the domain-wall dynamics are summarized in Fig. 6. Figure 6(a) shows the evolution of the total domain-wall length (L) for a number of values of δf that span the range of values that we studied. Figure 6(b) shows the evolution of the total domain area (A) for the same values of δf. In both cases, there is an obvious change in the time evolution as one changes δf. However, another weak effect is also apparent at early times: there is initially more domain-wall present for larger values of δf, suggesting smaller domains. This is not the focus of this work, but it is worth a brief comment.

The fact that a larger shift in frequency produces smaller initial domains makes qualitative sense. The ''nucleation'' of domains corresponds to the stabilization of standing wave patterns from an existing irregular state [14]. In the irregular state, there is a characteristic domain size and wavelength. Domains with the ''natural'' wavelength dominate, though a range of wavelengths are present. Therefore, this is not a classic nucleation from a perfectly uniform phase. As one changes the modulation frequency, regions with a wave number that matches the selected wave number will stabilize relatively quickly. As the shift in modulation frequency relative to the natural frequency increases, a smaller fraction of the pattern will have the ''correct'' wave number. Therefore, the initial size of the stabilized domains will be smaller.

As with the power spectra, we will use fits to power-law

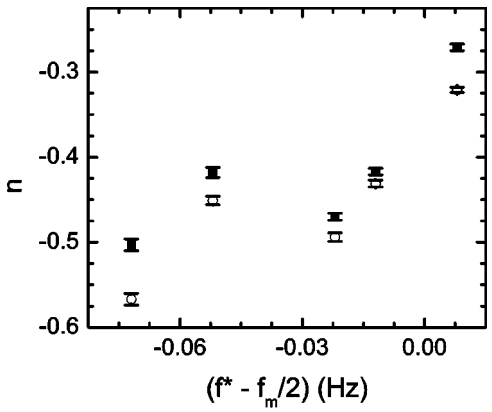

FIG. 7. Summary of measured scaling exponents (n) for both L (solid squares), and A (open circles).

growth to characterize the dynamics illustrated in Fig. 6. Unlike the power spectra, the measures of the domain-walls are not impacted by finite size effects during the time for which we studied the system. This is due to the fact that even though only a few domains are present in the system, there is still a significant amount of domain-wall. However, one still needs to be careful when interpreting these results. In studies of domain coarsening, it is standard to assume that a late-time scaling regime exists in which the lengths characterizing the domain size grow as a power law in time. One experimental difficulty with this assumption is determining when such a scaling regime is reached. This is especially true in the studies reported on here, where the average wave number is still evolving in time for all of the conditions that we studied (even if it is only logarithmic in time). Therefore, our focus is not on whether or not a true scaling regime has been reached. Instead, because the data is consistent with a power law of the form $L(t) \sim t^n$ and $A(t) \sim t^n$, we can use the values of n to compare the dynamics of the domain-walls under different circumstances. Any claims of a true scaling regime would be premature at this point, though the consistency of the data with power-law behavior suggests that it is possible that such a regime has been reached.

Figure 7 summarizes the results for the measured growth exponents n for both L and A. One observes that the evolution of the domains is significantly faster for larger $|\delta f|$, with n ranging from approximately 0.25–0.6. One also sees that the exponents for A and L are slightly different. The difference suggests an extremely slow decrease of the width in time, with $w \sim t^n$ and $n = -0.04 \pm 0.01$. By directly comparing A and L one finds that the change in the width is only ~ 0.2 pixels. This is consistent with the observation based on the images that the domain-wall width is essentially constant during the evolution. It should be noted that the evolution of the domain-wall width reported in Ref. [4] was also slow. However, in the simulations the domain-wall width grew in time, and we observe that, if anything, it shrinks in time.

IV. SUMMARY

The experiments reported on here demonstrate the close connection between the dynamics of domain-walls in pat-

terned systems and the evolution of the background wave number after a sudden change in the external parameters. We performed a series of quenches in which the steady-state average wave number after the quench is varied. The resulting evolution of the domain-walls depends on the steady-state value of $\langle k \rangle$. The rate of evolution for both the total domain-wall area and length increase as the wave number is varied away from its natural value.

Assuming A and L follow power-law scaling in time, exponents in the range of 0.25–0.6 are observed. As discussed in the Introduction, such a large variation in growth exponent is consistent with simulations of two different Swift-Hohenberg equations [1]. In Ref. [1], the calculated exponent is found to increase from 0.25 to 0.5 with a variation in wave number of approximately 20%. This difference in average wave number was suggested as the source of the different exponents. Though the agreement between our measurements and Ref. [1] is suggestive, it should be kept in mind that the simulations in Ref. [1] are for the *isotropic* Swift-Hohenberg equation and our system is *anisotropic*. Along these lines, it is interesting to compare the slow variation in the width of the domain-walls that we observed to the changes reported in Ref. [4]. Though opposite in sign, similar slow changes were observed in the simulations of an isotropic system [4]. These similarities between our results and simulations of isotropic systems may be due to the fact that the growth itself is relatively isotropic, as indicated by the evolution of the power spectrum parallel and perpendicular to the director (see Fig 5). At a minimum, the agreement between our results and simulations suggests that further work is needed to fully understand the impact of wave number variation on domain growth in patterned systems.

Finally, our results suggest that small modifications in the wave number of a pattern away from the natural wave number of the system can have a significant impact on the rate of growth of domains in the system. In our case, the maximum variation in wave number was only 6%, but the exponent changed from 0.25 to 0.6. If these results carry over to other patterned systems, such as diblock copolymers, one can have a relatively significant impact on the rate of growth of domains in systems where this has a practical impact on various processing applications [1,10].

ACKNOWLEDGMENTS

This work was supported by NSF Grant No. DMR-9975479. M. Dennin also thanks the Research Corporation and Alfred P. Sloan Foundation for additional funding for this work.

[1] M.C. Cross and D.I. Meiron, Phys. Rev. Lett. **75**, 2152 (1995).
[2] D. Boyer and J. Vinals, Phys. Rev. E **64**, 050101 (2001).
[3] H. Qian and G.F. Mazenko, e-print cond-mat/0210334.
[4] H. Qian and G.F. Mazenko, Phys. Rev. E **67**, 036102 (2003).
[5] C. Harrison, Z. Cheng, S. Sethuraman, D.A. Huse, P.M. Chaikin, D.A. Vega, J.M. Sebastian, R.A. Register, and D.H. Adamson, Phys. Rev. E **66**, 011706 (2002).
[6] C. Harrison, D.H. Adamson, Z. Cheng, J. Sebastian, S. Sethuraman, D. Huse, R.A. Register, and P.M. Chaikin, Science **290**, 1558 (2000).
[7] L. Purvis and M. Dennin, Phys. Rev. Lett. **86**, 5898 (2001).
[8] A.J. Bray, Adv. Phys. **43**, 357 (1994).
[9] K.R. Elder, J. Vinals, and M. Grant, Phys. Rev. Lett. **68**, 3024 (1992).
[10] J.J. Christensen and A.J. Bray, Phys. Rev. E **58**, 5364 (1998).
[11] D. Boyer and J. Vinals, Phys. Rev. E **65**, 046119 (2002).
[12] T. Taneike, T. Nihei, and Y. Shiwe, Phys. Lett. A **303**, 212 (2002).
[13] M. Dennin, D.S. Cannell, and G. Ahlers, Phys. Rev. E **57**, 638 (1998).
[14] M. Dennin, Phys. Rev. E **62**, 7842 (2000).
[15] P.G. de Gennes and J. Prost, *The Physics of Liquid Crystals* (Clarendon Press, Oxford, 1993).
[16] L. Kramer and W. Pesch, Annu. Rev. Fluid Mech. **27**, 515 (1995).
[17] M. Dennin, M. Treiber, L. Kramer, G. Ahlers, and D.S. Cannell, Phys. Rev. Lett. **76**, 319 (1996).
[18] U. Finkenzeller, T. Geelhaar, G. Weber, and L. Pohl, Liq. Cryst. **5**, 313 (1989).
[19] E.H.C.CO., Ltd., 1164 Hino, Hino-shi, Tokyo, Japan.
[20] M. Dennin, Phys. Rev. E **62**, 6780 (2000).
[21] S. Rasenat, G.H.B.L. Winkler, and I. Rehberg, Exp. Fluids **7**, 412 (1989).
[22] M. Dennin, D.S. Cannell, and G. Ahlers, Science **272**, 388 (1996).
[23] D.A. Egolf, I.V. Melnikov, and E. Bodenschatz, Phys. Rev. Lett. **80**, 3228 (1998).
[24] IMAQ Vision package is a product of National Instruments.